Bi3+ Effects on Down-/up-conversion Luminescence, Temperature Sensing and Optical Transition Properties in Bi3+/Er3+ Co-doped YNbO4 Phosphors

Xin Wang
Dalian Maritime University
Xiangping Li
Dalian Maritime University
Hongquan Yu
Dalian Maritime University
Sai Xu
Dalian Maritime University
Jiashi Sun
Dalian Maritime University
Lihong Cheng
Dalian Maritime University
Xizhen Zhang
Dalian Maritime University
Jinsu Zhang
Dalian Maritime University
Yongze Cao
Dalian Maritime University
Baojiu Chen (chenmbj@souhu.com)
aSchool of Science, Dalian Maritime University, Dalian, Liaoning, 116026, PR China

Research Article

Keywords: YNbO4, Bi3+/Er3+, Down-conversion luminescence, Up-conversion luminescence, Temperature sensing

Posted Date: September 17th, 2020

DOI: https://doi.org/10.21203/rs.3.rs-76690/v1

Bi^{3+} effects on down-/up-conversion luminescence, temperature sensing and optical transition properties in Bi^{3+}/Er^{3+} co-doped $YNbO_4$ phosphors

Xin Wang, Xiangping Li[1], Hongquan Yu, Sai Xu, Jiashi Sun, Lihong Cheng, Xizhen Zhang, Jinsu Zhang, Yongze Cao, Baojiu Chen*

[a]School of Science, Dalian Maritime University, Dalian, Liaoning, 116026, PR China

Abstract

A series of Bi^{3+} single-doped and Bi^{3+}/Er^{3+} co-doped $YNbO_4$ phosphors with various concentrations of Bi^{3+} ions were prepared by a conventional high temperature solid-state reaction method. The results of XRD and Rietveld refinement confirmed that monoclinic phase $YNbO_4$ samples were achieved. The down-/up-conversion luminescence of Er^{3+} ions were investigated under the excitation of ultraviolet light (327 nm) and near infrared light (980 nm). Under 327 nm excitation, broad visible emission band from Bi^{3+} ions and characteristic green emission peaks from Er^{3+} ions were simultaneously observed, while only strong green emissions from Er^{3+} ions were detected upon excitation of 980 nm. Remarkable emission enhancement was observed in down-/up-conversion luminescence processes by introducing Bi^{3+} ions into Er^{3+}-doped $YNbO_4$ phosphors. By analyzing the laser working current dependent up-conversion luminescence spectra, two-photon processes were confirmed to be responsible for both the green and the red up-conversion emissions of Er^{3+} ion. The temperature sensing property of Er^{3+} was studied by using the temperature dependent up-conversion luminescence spectra and it was found that the temperature sensitivity was sensitive to the doping concentration of Bi^{3+} ions. By comparing the experimental

[1] E-mail: lixp@dlmu.edu.cn (Li XP) & chenmbj@souhu.com (Chen BJ)

values of the radiative transition rate ratio of the two green emission levels of Er^{3+} ions and the theoretical values calculated by Judd-Ofelt (J-O) theory, it was concluded that energy level splitting had significant influences on the temperature sensing property of Er^{3+} ions.

Keywords: $YNbO_4$: Bi^{3+}/Er^{3+}; Down-conversion luminescence; Up-conversion luminescence; Temperature sensing

1. Introduction

With the rapid development of modern technology, rare earth (RE^{3+}) ions doped luminescent materials have evoked great attention because of their potential and practical applications in solid-state lighting, optical imaging, temperature sensors, color displays and so on [1-4]. Among numerous RE^{3+} ions, Er^{3+} ion is considered to be an excellent green emitting center in down-/up-conversion (DC/UC) luminescence materials thanks to its predominant ($^2H_{11/2}$, $^4S_{3/2}$) $\rightarrow$$^4I_{15/2}$ transitions [5]. Moreover, these two green-emitting energy levels $^2H_{11/2}$, $^4S_{3/2}$ are thermally coupled energy levels, whose populations fulfill Boltzmann's distribution law. The fluorescence intensity ratio (*FIR*) of the two green emissions depends on the sample temperature, Er^{3+} ion has been extensively studied as an optical temperature sensing unit [6-8]. Compared with traditional contact temperature detection devices, this kind of optical temperature sensor based on *FIR* technique exhibits higher resolution and can realize non-contact and real-time temperature sensing in harsh environments [9, 10].

In general, the host matrix has significant effects on the optical properties of the luminescent materials. $LnNbO_4$ (Ln = La, Gd, Y) compounds, as a type of niobates,

have been investigated as RE^{3+}-doped DC/UC luminescent materials owing to their excellent chemical property, good thermal stability, and lower phonon energy than the most other oxide compounds [11-13]. $YNbO_4$, as a self-activated phosphor, exhibits an efficient blue emission upon 254 nm excitation [14], white-light-emitting has been realized in a single composition $YNbO_4$: Eu^{3+}, Tb^{3+} phosphor by tuning the relative doping concentrations of Eu^{3+} and Tb^{3+} [14].

It is well known that adding proper sensitizers in the luminescent materials can improve the optical performance of the activators [15, 16]. Bi^{3+} ion, as a good sensitizer, has been adopted as co-dopant in many RE^{3+}-doped DC luminescent materials and significant enhancements in the emission intensities of Er^{3+}, Eu^{3+} and Dy^{3+} ions have been achieved [17-19]. Additionally, remarkable enhancement of UC luminescence of RE^{3+} (RE=Er, Tm, Ho) was also observed in fluoride materials via adjusting the host lattice and the local crystal field by co-doping of Bi^{3+} ions [20]. Er^{3+}-doped $YNbO_4$ is a good phosphor from which the green emissions can be obtained under both DC and UC excitation conditions. In order to improve the luminescence performances of Er^{3+} ions in $YNbO_4$ samples, Bi^{3+}/Er^{3+} co-doped phosphors were prepared and the luminescence properties were systematically studied.

Building from the above ideas, in the present work, Bi^{3+}/Er^{3+} co-doped $YNbO_4$ phosphors were synthesized using a high temperature solid-state reaction method. The influence of Bi^{3+} concentration on the DC/UC luminescence properties of Er^{3+} ions was studied. In the presence of Bi^{3+} ions, significant enhancements in the emission

intensities of Er^{3+} ions in both DC and UC luminescence processes were observed. Moreover, the temperature sensing properties of Bi^{3+}/Er^{3+} co-doped $YNbO_4$ phosphors were also studied. The effect of energy level splitting on the temperature sensitivity and optical transition properties were discussed based upon the framework of Judd-Ofelt (J-O) theory.

2. Experimental

A series of Bi^{3+} single-doped and Bi^{3+}/Er^{3+} co-doped $YNbO_4$ powder phosphors were prepared via a traditional high temperature solid-state reaction method. Er^{3+} concentration was fixed as 5.0 mol%, and Bi^{3+} concentrations (x mol%) were designed to be 0, 0.5, 1.0, 3.0, and 5.0 mol%, respectively. In a typical synthesis procedure, the raw materials Y_2O_3 (99.99%), Bi_2O_3 (99.99%), Er_2O_3 (99.99%) and Nb_2O_5 (99.99%) were weighed on the basis of stoichiometric ratio and well ground with the help of an agate mortar and pestle. After homogeneous mixing, these mixtures were transferred into alumina crucibles and placed into a programmed muffle furnace at room temperature. The furnace was heated from room temperature to 1300 ℃ within 2 h, and these mixtures were kept at 1300 ℃ for 4 h. Lastly, the products were obtained after the furnace-cooled naturally to room temperature.

X-ray diffraction (XRD) measurements were carried out by a powder diffractometer (SHIMADZU, XRD-6000, Japan) operating at 40 kV and 30 mA with $CuK\alpha_1$ radiation (λ = 0.15406 nm). The continuous-scanning mode with a scanning rate of 4°/min was adopted for phase identification with a 2θ range from 20° to 70°. The DC luminescence spectra were recorded by a Hitachi F-4600 fluorescent

spectrometer equipped with a built-in excitation source (150 W Xenon lamp). The UC luminescence spectra were measured by the same spectrometer assisted by an external power-controllable 980 nm fiber laser. The temperature of the samples was adjusted by a homemade temperature controlling system, DMU-TC 450, which was composed by a small stove and an intelligent digital-display-type temperature control instrument. The controlling accuracy for temperature was about ± 0.5 ℃. The diffuse-reflection spectrum was collected by a spectrophotometer (Shimadzu, UV-3600, Japan) equipped with an integrating sphere accessory, and $BaSO_4$ powder was used as the reference.

3. Results and discussion

3.1 Crystal structure

The phase identification of the as-synthesized samples was examined by XRD measurement. Fig. 1 shows the XRD patterns of 5.0 mol% Bi^{3+} single-doped and 5.0 mol% Er^{3+}/*x* mol% Bi^{3+} (*x* = 0, 1.0, and 5.0) co-doped $YNbO_4$ powders as well as the standard pattern of monoclinic $YNbO_4$ reported in JCPDS No. 83-1319. It can be seen that all the diffraction peaks of the as-synthesized samples are in accordance with the standard data. No extra peak corresponding to any other impurity is observed even in the samples with higher doping concentrations of Bi^{3+} or Er^{3+} ions.

<<Fig. 1 around here>>

To better describe the variation of the crystal lattice parameters of $YNbO_4$ samples after introducing various concentrations of Er^{3+} and Bi^{3+} ions, Rietveld refinements were performed by using the general structure analysis system (GSAS)

program [21, 22]. The refinement results are depicted in Fig. 2 and the corresponding lattice parameters are listed in Table 1. As can be seen in Fig. 2, all the diffraction peaks are fitted well with the Rietveld theoretical model. The residual factors (R_{WP}, R_P, and χ^2) of the refinement converged to an acceptable level, implying that the refinements are reliable. Thus, it can be concluded that all the as-synthesized $YNbO_4$ samples are of monoclinic phase. From Table 1, it can be found that the lattice constants increase with the increase of Bi^{3+} concentration, indicating the host lattice dimension expands after Bi^{3+} doping. This may be caused by the substitution of Y^{3+} (0.90 Å) sites by the larger Bi^{3+} ion (1.03 Å) [23]. It is reported that such substitution can tailor the local crystal field around Er^{3+} ions in the host lattice, which may have effects on the UC luminescence property of Er^{3+} ions [24].

<<Fig. 2 around here>>

<<Table. 1 around here>>

3.2 Luminescence properties of Bi^{3+} single-doped $YNbO_4$ phosphors

Fig. 3(a) shows the excitation and emission spectra of Bi^{3+} single-doped $YNbO_4$ phosphors. The excitation spectrum monitored at 437 nm only consists of a broad excitation band in the range of 200 to 350 nm, which is attributed to the spin-allowed $^1S_0 \rightarrow {}^3P_1$ transition of Bi^{3+} ions and the absorption of NbO_4^{4-} [12, 25]. Upon 327 nm excitation, Bi^{3+} single-doped sample exhibits blue emission and only a broad band extending from 350 nm to 625 nm can be observed, which originates from the characteristic transition $^3P_1 \rightarrow {}^1S_0$ of Bi^{3+} ions [26]. The emission spectra of the samples doped with various concentrations of Bi^{3+} ions (x = 0.5, 1.0, 3.0 and 5.0)

excited at 327 nm were measured and the results are depicted in Fig. 3(b). It can be seen that the emission intensity increases with the augment of Bi^{3+} concentration, and then starts to decline when Bi^{3+} concentration reaches a maximum value at 3.0 mol% because of concentration quenching.

<<Fig. 3 around here>>

3.3 Luminescence properties of Er^{3+}/Bi^{3+} co-doped $YNbO_4$ phosphors

Fig. 4 presents the typical excitation and emission spectra for 5.0 mol% Bi^{3+}, 5.0 mol% Er^{3+} single-doped and co-doped $YNbO_4$ samples. For Bi^{3+} single-doped $YNbO_4$ phosphor, the excitation and emission spectra are in agreement with the above results shown in Fig. 3. As depicted in Fig. 4(b), it can be seen that the excitation spectrum of Er^{3+} single-doped $YNbO_4$ sample monitored at 555 nm (corresponding to the $^4S_{3/2} \rightarrow {}^4I_{15/2}$ transition of Er^{3+} ions) consists of two parts. One is a broad excitation band centered at around 265 nm, which can be assigned to the absorption of NbO_4^{4-} [7]. The other part comprises of some sharp peaks located in the wavelength region from 350 nm to 600 nm, corresponding to the characteristic 4*f*-4*f* transitions from the ground state $^4I_{15/2}$ level to the excited states $^4G_{11/2}$, $^2H_{9/2}$, $^4F_{3/2}$, $^4F_{5/2}$, and $^2H_{11/2}$ levels of Er^{3+}, respectively. Under 379 nm excitation, only green emissions can be detected, which are originated from the characteristic transitions ($^2H_{11/2}$, $^4S_{3/2}$) $\rightarrow {}^4I_{15/2}$ of Er^{3+} ions. Obviously, Fig. 4(a) and (b) reveal a wide spectral overlap between the emission spectrum of Bi^{3+} ion and the excitation spectrum of Er^{3+} ion, which indicates that effective energy transfer from Bi^{3+} to Er^{3+} is expected in Bi^{3+}/Er^{3+} co-doped $YNbO_4$ phosphors [27]. This energy transfer process can also be proved by the excitation and

emission spectra of Bi^{3+}/Er^{3+} co-doped $YNbO_4$ phosphors. As shown in Fig. 4(c), by monitoring the emission at 555 nm, the excitation spectrum of Bi^{3+}/Er^{3+} co-doped sample is composed of a broad excitation band of Bi^{3+} ion as well as the 4*f*-4*f* transitions of Er^{3+} ion. Moreover, upon the excitation of 327 nm, the emission spectrum of Bi^{3+}/Er^{3+} co-doped sample contains not only the broad emission band from Bi^{3+} ions but also the characteristic emission peaks from Er^{3+} ions. The above results indicate that the introduction of Bi^{3+} ions greatly extends the excitation band range of Er^{3+}-doped $YNbO_4$ phosphors in near-ultraviolet light region, which is benefit for the application in ultra-violet excited white light emitting diodes.

<<Fig. 4 around here>>

Fig. 5 depicts the emission spectra of $YNbO_4$: Er^{3+} phosphors doped with various concentrations of Bi^{3+} ions excited at 327 nm ($^1S_0 \rightarrow {}^3P_1$ transition of Bi^{3+}). It can be seen that all the emission spectra are similar and each of them consists of a strong emission band from Bi^{3+} ion and some sharp emission peaks from Er^{3+} ion. It is noteworthy that there are two weak absorption peaks in the broad emission band, which can be ascribed to the absorption transitions $^4I_{15/2} \rightarrow {}^4F_{5/2}$, $^4I_{15/2} \rightarrow {}^4F_{7/2}$ of Er^{3+} ion. This result demonstrates that part of the emissions from Bi^{3+} ions is reabsorbed by Er^{3+} ions. With the increase of Bi^{3+} concentration, both of the intensities of the broad emission band of Bi^{3+} ions and the green emission peaks of Er^{3+} ions enhance gradually first and reach the strongest values at 3.0 mol% Bi^{3+} co-doped case, after which the intensities begin to decline with further increasing the concentration of Bi^{3+} ions. The intensification of the intensity at low Bi^{3+} doping case can be ascribed to the

enhancement of the interaction between Bi^{3+} and Er^{3+} ions caused by the shorten distance between them as Bi^{3+} concentration rising, while the attenuation of the emissions at higher Bi^{3+} doping case is probably due to the concentration quenching effect, which mainly results from non-radiative energy transfer among the activators [26].

Chromatic property is one of the important parameters for evaluating the phosphors' performance. According to the intensity-calibrated emission spectra, the Commission International de I' Eclairage in 1931 (CIE 1931) color coordinates of the samples were calculated and are shown in the inset of Fig. 5, it can be seen that the color coordinates of Er^{3+}/Bi^{3+} co-doped samples are mainly located in the blue light region due to the strong emission from Bi^{3+} ions.

<<Fig. 5 around here>>

Fig. 6 shows the UC emission spectra of Er^{3+}/Bi^{3+} co-doped $YNbO_4$ phosphors upon excitation of 980 nm measured at room temperature. As can be seen, only typical green and red UC emission peaks belonging to the characteristic 4*f*-4*f* transitions of Er^{3+} ions can be observed, no peak related to Bi^{3+} ion is detected. And the doping of Bi^{3+} ions does not cause obvious change of the position and the shape of the emission peaks of Er^{3+} ions. However, significant enhancement of the emission intensities of Er^{3+} ions was observed after Bi^{3+} doping. The inset of Fig. 6 shows the dependence of the integrated intensities of both green and red UC emissions of Er^{3+} ions on Bi^{3+} concentrations. It can be seen that the variation trends of the green and the red UC emissions are identical. Both of them increase with the increase of Bi^{3+}

concentration and achieve their maximum values when Bi^{3+} concentration reaches at 3.0 mol%, after which the emission intensities decrease.

<<Fig. 6 around here>>

To provide more in depth understanding of the UC luminescence mechanism of Er^{3+} ions in Er^{3+}/Bi^{3+} co-doped $YNbO_4$ phosphors, the UC emission spectra of the samples doped with various concentrations of Bi^{3+} ions as a function of pumped power (P) were examined under 980 nm excitation. It is well known that for a n-photon UC luminescence process (n is the number of required photon), the UC emission intensity (I_{up}) is proportional to P^n, which can be expressed as $I_{up} = MP^n$ (M is a constant) [28]. To determine the values of n, the integral intensities of the green and the red UC emissions were recorded and the dependence of them on the pumped power density are shown in Fig. 7. It can be seen that the intensities of both the green and the red UC emissions increase as the pumped power density rising. Then, the data were fitted by using the aforementioned equation and the fitting results are also shown in Fig. 7, denoted as solid lines. It is confirmed that the n values of both the green and the red UC emissions are all around 2, meaning that two-photon processes are responsible for both the green and the red UC emissions no matter what the concentration of Bi^{3+} ion is. The detailed UC luminescence processes are similar with those reported results and can be referred to Ref. [29].

<<Fig. 7 around here>>

From the above-mentioned excitation and emission spectra, it has been found that Bi^{3+} ion possesses a broad absorption band around 327 nm and a broad emission

band extending from 350 nm to 625 nm. No absorption of Bi^{3+} ion at around 980 nm was observed [30], thus Bi^{3+} ion cannot absorb 980 nm excitation energy and there is no energy transfer from Bi^{3+} ions to Er^{3+} ions upon 980 nm excitation. Meanwhile, because no emission from Bi^{3+} ion was found in the UC emission spectra, there is no energy transfer from Er^{3+} ions to Bi^{3+} ions either. Therefore, energy transfer is not the reason for the enhancement of UC luminescence of Er^{3+} ions by introducing Bi^{3+} ions.

According to the quantum selection rules, the intra-4*f* electronic transitions of RE^{3+} ions are parity forbidden and strongly depend on the local crystal field and site symmetry, which can be partially broken when RE^{3+} ions situate at low symmetry sites [17, 20, 31]. Because the radius of Bi^{3+} ion is different from that of Y^{3+} ion, the crystal field environment around Er^{3+} ion may be modified when Y^{3+} sites are substituting by Bi^{3+} ions, which may induce the change of the radiative transition rate and affect the UC emission intensity of Er^{3+} ions. Zhang et al. have theoretically illustrated that significant UC luminescence enhancement of Er^{3+} ion arises from the synthesized tailoring effect induced by the Li^{+} ions [24]. Thus, it is considered that the modification of the local crystal field environment around Er^{3+} ions via Bi^{3+} doping is the main reason for the enhancement of UC luminescence intensity of Er^{3+} ions. Similar results were also observed in Er^{3+}, Yb^{3+}, Bi^{3+} tri-doped $NaYF_4$ crystals [20]. Moreover, When the doping concentration of Bi^{3+} ion exceeds 3.0 mol%, the excessive Bi^{3+} ions will enlarge the distance between Er^{3+} ions and weaken the interaction between them and then induce the decrease of the emission intensities of Er^{3+} ions.

3.4 Temperature sensing properties of $YNbO_4$: Er^{3+}/Bi^{3+} phosphors

To investigate the temperature dependent luminescence behavior of the prepared phosphors with different Bi^{3+} concentrations, the temperature-varied emission spectra were measured in the temperature region of 303-573 K under 980 nm excitation with the pumping power density of 24.84 W/cm^2, and the results are shown in Fig. 8. It can be seen that the intensities of both the two green emissions came from $^2H_{11/2}\rightarrow{}^4I_{15/2}$ and $^4S_{3/2}\rightarrow{}^4I_{15/2}$ transitions of Er^{3+} ions decrease as an increase in sample temperature. According to the temperature-varied UC luminescence spectra, the *FIRs* of the two green emissions were calculated based upon their integral intensities obtained by Gaussian fitting. As representatives, Fig. 9 shows the relationship between the *FIR* of the two green emissions and the sample temperature for $YNbO_4$: Er^{3+} samples doped with *x* mol% Bi^{3+} (*x* = 0, 1.0, 3.0 and 5.0). It is apparent that the *FIR*s of all samples monotonically increase as temperature rising.

It is well known that $^2H_{11/2}$ and $^4S_{3/2}$ levels of Er^{3+} ions belong to thermally coupled energy levels, whose population numbers follow Boltzmann's distribution law, thus the *FIR* of the two green emissions can be expressed as [32]:

$$R(T)=\frac{I_H}{I_S}=\frac{A_H N_H}{A_S N_S}=\frac{A_H \exp(-E_H/kT)}{A_S \exp(-E_s/kT)}=\frac{A_H}{A_S}\exp\left(\frac{-\Delta E}{kT}\right) \quad (1)$$

where I_H, I_S, N_H, N_S, and A_H, A_S are the integral fluorescence intensities, the population numbers, and the radiative transition rate of the emissions from $^2H_{11/2}\rightarrow{}^4I_{15/2}$ and $^4S_{3/2}\rightarrow{}^4I_{15/2}$ transitions, respectively. ΔE, k, and T are the energy distance between $^2H_{11/2}$ and $^4S_{3/2}$ levels, Boltzmann's constant and absolute temperature, respectively. All the experimental data shown in Fig. 9 are fitted by Eq. (1) and the solid and

dashed lines represent the fitting results. As can be seen, the experimental data are fitted well by Eq. (1). Moreover, in the fitting processes, the values of A_H/A_S and $\Delta E/T$ were obtained, and the confirmed equations for all samples are also exhibited in Fig. 9. It can be found that the values of A_H/A_S decline with the increase of Bi^{3+} concentration.

<<Fig. 8 around here>>

<<Fig. 9 around here>>

Usually, the temperature sensitivity ($S(T)$) can be defined as the rate of change of R per unit temperature, and $S(T)$ of Er^{3+}-based temperature sensor can be mathematically expressed as [33]:

$$S(T) = \frac{dR(T)}{dT} = \frac{A_H}{A_S}\exp\left(\frac{-\Delta E}{kT}\right)\left(\frac{\Delta E}{kT^2}\right) \quad (2)$$

By taking the above obtained values of A_H/A_S and $\Delta E/k$ into Eq. (2), the sensitivity function $S(T)$ versus T for the phosphors all samples were calculated and the corresponding temperature sensitivity curves are shown in Fig. 10. It can be seen that the variation of the temperature sensitivity is quite similar for all samples. The sensitivity first increases with the increase of temperature, until it reaches the maximum value, then it slowly decreases with further increase of temperature. And the sample in absence of Bi^{3+} ions has the highest temperature sensing sensitivity.

<<Fig. 10 around here>>

3.5 Judd-Ofelt analysis of $YNbO_4$: Er^{3+}/Bi^{3+} phosphors

According to the results of temperature sensing property, it can be found that the concentration of Bi^{3+} ion has significant effects on the value of A_H/A_S and the

temperature sensing sensitivity of Er^{3+} ions. As Bi^{3+} concentration rising, both of them decrease dramatically. It is well known that J-O theory provides a helpful method to investigate the optical transition properties of RE^{3+}-doped luminescent materials, including radiative transition rates, fluorescence branching ratios, quantum efficiencies and so on [34, 35]. On the basis of this theory, the influence of the local matrix environment on the optical transition properties of Er^{3+} ion in $YNbO_4$: Er^{3+}/Bi^{3+} samples were discussed more in-depth and theoretical. The J-O parameters of Er^{3+} and Sm^{3+} single-doped powder samples have been calculated by J-O theory before and the detailed calculation process can be referred to Refs. [36-38].

To obtain the J-O parameters of Er^{3+} ion in $YNbO_4$: Er^{3+}/Bi^{3+} powders, the diffuse reflection spectra of *x* mol% Bi^{3+} (*x* = 0, 1.0, 3.0 and 5.0) doped $YNbO_4$: Er^{3+} samples were measured under the same experimental conditions in the wavenumber of 2000-30000 cm^{-1}. According to the Kubelka-Munk (K-M) function [39], the relative absorption cross-section spectra of these samples were derived, and the results are shown in Fig. 11. All the relative absorption cross-section spectra exhibit similar spectral profile, all of them include eleven bands corresponding to the absorption transitions from the ground state $^4I_{15/2}$ to the excited states $^4I_{13/2}$, $^4I_{11/2}$, $^4I_{9/2}$, $^4F_{9/2}$, $^4S_{3/2}$, $^2H_{11/2}$, $^4F_{7/2}$, $^4F_{5/2}/F_{3/2}$, $^2H_{9/2}$, $^4G_{11/2}$ and $^4G_{7/2}/^4G_{9/2}/\ ^2K_{15/2}$ of Er^{3+} ion, respectively. Based on the relative absorption spectra, the relative J-O parameters Ω'_λ (λ = 2, 4, 6) of $YNbO_4$: Er^{3+}/Bi^{3+} powder samples were calculated and the results are shown in Table 2. Then, the relative electric dipole transition rate $A'^{ed}_{^4I_{13/2}\rightarrow{}^4I_{15/2}}$ of $YNbO_4$: Er^{3+} powder samples doped with *x* mol% Bi^{3+} (*x* = 0, 1.0, 3.0 and 5.0) were obtained to be

3.12, 6.06, 7.62, and 9.63 s^{-1}, respectively.

<<Fig. 11 around here>>

<<Table. 2 around here>>

As is well known, the lifetime for a level is reciprocal to its radiative transition rate. Thus, the real J-O parameters of $YNbO_4$: Er^{3+}/Bi^{3+} powders can be calibrated by the fluorescence decay of $^4I_{13/2}$ level of Er^{3+} ions. As labeled in Fig. 12, it can be seen that the fluorescence decay curve of Er^{3+} ion in $YNbO_4$: 0.5 mol% Er^{3+} phosphor can be well linearly fitted in the semi-logarithmic coordinate system, and the fitting result shows that the lifetime of $^4I_{13/2}$ level of Er^{3+} ion is 4.53 ms. The relationship between the lifetime of $^4I_{13/2}$ level and its radiative transition rate can be expressed as $\frac{1}{\tau_{^4I_{13/2}}} = A_{^4I_{13/2}\rightarrow{}^4I_{15/2}} = A^{ed}_{^4I_{13/2}\rightarrow{}^4I_{15/2}} + A^{md}_{^4I_{13/2}\rightarrow{}^4I_{15/2}}$. The value of $A^{md}_{^4I_{13/2}\rightarrow{}^4I_{15/2}}$ can be calculated to be 89.45 s^{-1} according to the following formula: $A^{md}_{L\rightarrow L'} = \frac{16\pi^4 e^2 n^3}{3h(2J+1)m^2c^2}\left|\langle \Psi J \| L+2S \| \Psi' J' \rangle\right|^2$. Then, the real electric radiation transition rate $A^{ed}_{^4I_{13/2}\rightarrow{}^4I_{15/2}}$ was calculated to be 131.30 s^{-1}, and the proportional coefficient between $A'^{ed}_{^4I_{13/2}\rightarrow{}^4I_{15/2}}$ and $A^{ed}_{^4I_{13/2}\rightarrow{}^4I_{15/2}}$ of $YNbO_4$: Er^{3+}/x mol% Bi^{3+} (x = 0, 1.0, 3.0 and 5.0) powders were obtained to be 42.08, 21.67, 17.23, and 13.63, respectively. Therefore, the real J-O parameters Ω_λ (λ = 2, 4, 6) can be obtained via multiplying the relative values by the corresponding proportional coefficients, and the results are also shown in Table 2. As can be seen, Ω_2 value decreases as the increase of Bi^{3+} concentration, while the values of Ω_4 and Ω_6 only have a little change. Typically, among the J-O parameters Ω_λ (λ = 2, 4, 6), Ω_2 parameter is associated with

short-range coordination effects and strongly depends on the local environment, the other two parameters Ω_4 and Ω_6 depend on long-range effects [40, 41].

<<Fig. 12 around here>>

Based on these modified J-O parameters, the real electric dipole radiation transition rate $A^{ed}_{^4I_{13/2}\rightarrow{}^4I_{15/2}}$ for $YNbO_4$: Er^{3+}/Bi^{3+} powders can be calculated accordingly. And then the theoretical values of A_H/A_S were derived and the results are shown in Table 3, accompanying with the aforementioned experimental results to make a comparison. As can be seen, the value of A_H/A_S is sensitive to the doping concentration of Bi^{3+} ions, and with the increase of Bi^{3+} concentration the value of A_H/A_S decreases, which has the same change trend as the previous experimental results. However, the calculated values of A_H/A_S are a little larger than the experimental ones. Because the spectra of the two green emissions have line-width and only the *FIR* value of the barycenter wavenumber of each energy level is considered in the theoretical formula Eq. (1), therefore, errors may be introduced in the experimental values. In addition, obvious energy levels splitting of the two thermally coupled energy levels of Er^{3+} ions have been observed in Fig. 8, the population of these two levels may not in good agreement with the Boltzmann's distribution law. Thus, Eq. (1) may not accurately describe the relationship between the value of *FIR* of the two green emissions and sample temperature.

<<Table. 3 around here>>

As can be seen from Fig. 13, the spectrum from ($^2H_{11/2}$, $^4S_{3/2}$) $\rightarrow{}^4I_{15/2}$ transitions of Er^{3+} ion can be divided into four peaks by Gaussian fitting. The solid circles are the

experimental data, the solid and the dotted lines are the Gaussian fitting curves. Here we only consider the splitting of the excited state levels caused by the interaction of crystal field. The results indicate that the two green emission levels split into four sub-levels, which are named as $^2H_{11/2(1)}$, $^2H_{11/2(2)}$, $^4S_{3/2(1)}$, and $^4S_{3/2(2)}$, respectively. Considering the populations of each two sub-levels also follow the Boltzmann's distribution law, the *FIR* of the two green emissions can be modified as:

$$R'(T)=\frac{I_{H1}+I_{H2}}{I_{S1}+I_{S2}}=\frac{A_{H1}\exp(-E_{H1}/kT)+A_{H2}\exp(-E_{H2}/kT)}{A_{S1}\exp(-E_{S1}/kT)+A_{S2}\exp(-E_{S2}/kT)}=\frac{A_{H1}/A_{S2}\exp(-\Delta E_{H1\text{-}S2}/kT)+A_{H2}/A_{S2}\exp(-\Delta E_{H2\text{-}S2}/kT)}{A_{S1}/A_{S2}\exp(-\Delta E_{S1\text{-}S2}/kT)+1} \quad (3)$$

where I_{H1}, I_{H2}, I_{S1}, I_{S2}, and A_{H1}, A_{H2}, A_{S1}, A_{S2} are the integrated fluorescence intensities and the radiative transition rate of the emissions from $^2H_{11/2(1)}\rightarrow{}^4I_{15/2}$, $^2H_{11/2(2)}\rightarrow{}^4I_{15/2}$, $^4S_{3/2(1)}\rightarrow{}^4I_{15/2}$ and $^4S_{3/2(2)}\rightarrow{}^4I_{15/2}$ transitions, respectively. $\Delta E_{H1\text{-}S2}$, $\Delta E_{H2\text{-}S2}$ and $\Delta E_{S1\text{-}S2}$ are the energy distance between $^2H_{11/2(1)}$, $^2H_{11/2(2)}$, $^4S_{3/2(1)}$ and $^4S_{3/2(2)}$ levels, respectively. Eq. (3) was used to fit the data depicted in Fig. 9 and the results are shown in Fig. 14 along with the confirmed equations. It can be seen that all the experimental data can be fitted well by Eq. (3). All of the values of $\Delta E_{H1\text{-}S2}/k$, $\Delta E_{H2\text{-}S2}/k$ and $\Delta E_{S1\text{-}S2}/k$ are respectively around 1460.0, 1010.0 and 500.0. The corresponding $\Delta E_{H1\text{-}S2}$, $\Delta E_{H2\text{-}S2}$ and $\Delta E_{S1\text{-}S2}$ values are 1014.1 cm^{-1}, 701.5 cm^{-1} and 347.3 cm^{-1}, which are in good agreement with the values (1032.6 cm^{-1}, 714.4 cm^{-1} and 352.0 cm^{-1}) obtained from the measured UC luminescence spectra. This fact suggests that Eq. (3) can well explain the temperature dependence of *FIR* of the two green emissions. The above results show that the Boltzmann's law must be used carefully to study the temperature sensing characteristics of Er^{3+} ions in the case of energy level splitting. This is also the reason why the deviation from theoretical to experimental

values in Table 3 is existent.

<<Fig. 13 around here>>

<<Fig. 14 around here>>

4. Conclusion

Er^{3+}, Bi^{3+} co-doped $YNbO_4$ phosphors were successfully synthesized via a high temperature solid-state reaction method. Co-doping Bi^{3+} ions enhanced the emission intensities of Er^{3+} ions in $YNbO_4$: Er^{3+}/*x* mol% Bi^{3+} (*x* = 0, 0.5, 1.0, 3.0, and 5.0) phosphors under both 327 and 980 nm excitations. The former enhancement can be ascribed to the efficient energy transfer from Bi^{3+} ions to Er^{3+} ions, while the latter one was caused by the modification of the local crystal field environment around Er^{3+} ions via Bi^{3+} doping. By studying the excitation power density dependent UC luminescence spectra, it was confirmed that 2-phonton processes were dominated in both of the green and the red UC emissions. According to the temperature sensitivity curves, it was confirmed that the lower concentration of Bi^{3+} ions, the higher temperature sensitivity of the $YNbO_4$: Er^{3+}/Bi^{3+} samples. In addition, the optical transition property of Er^{3+} ion was investigated within the framework of J-O theory, and the results showed that the doping concentration of Bi^{3+} ions and the energy level splitting of $^2H_{11/2}$ and $^4S_{3/2}$ levels of Er^{3+} ions had effects on the temperature sensing property of Er^{3+} ions.

Author contribution statement

Xin Wang: Carrying out experiments, Data curation, Writing-original draft. Xiangping Li and Baojiu Chen: Conceptualization, Supervision, Writing-review &

editing. Hongquan Yu and Lihong Cheng: Formal analysis. Sai Xu: Software. Jiashi Sun: Methodology. Xizhen Zhang, Jinsu Zhang and Yongze Cao: Investigation, Approval.

Declaration of competing interest

The authors declare that they have no known competing financial interests or personal relationships that could have appeared to influence the work reported in this paper.

Acknowledgements

This work was partially supported in part by the NSFC (National Natural Science Foundation of China, Grant Nos. 11774042 and 11704056), in part by the Postgraduate Education and Teaching Reform Project of Dalian Maritime University (Nos. YJG2019210 and YJG2019209), in part by the Fundamental Research Funds for the Central Universities (Grant Nos. 3132020177 and 3132019338) and in part by the Open Fund of the State Key Laboratory of Integrated Optoelectronics granted (No. IOSKL2019KF06).

References

[1] Choudhary AK, Dwivedi A, Bahadur A, et al. Enhanced upconversion emission and temperature sensor sensitivity in presence of Bi^{3+} ions in Er^{3+}/Yb^{3+} co-doped $MgAl_2O_4$ phosphor. *Ceram. Int.* 2018, **44**: 9633-9642.

[2] Jiang L, Xiao S, Yang X, et al. Enhancement of up-conversion luminescence in Zn_2SiO_4:Yb^{3+}, Er^{3+} by co-doping with Li^+ or Bi^{3+}. *Appl. Phys. B* 2012, **107**: 477-481.

[3] Dey R, Kumar Rai V. Er^{3+}-Tm^{3+}-Yb^{3+}: $CaMoO_4$ phosphor as an outstanding

upconversion-based optical temperature sensor and optical heater. *Methods Appl Fluoresc* 2017, **5**: 015006-015011.

[4] Shuang FL, Robert R, William SR, et al. In vivo and scanning electron microscopy imaging of up-converting nanophosphors in caenorhabditiselegans. *Nano Lett.* 2006, **6**: 169-170.

[5] Capobianco IA, Prevost G, Proulx PP, et al. Upconversion properties of Er^{3+} doped lead silicate glasses. *Opt. Mater.* 1996, **6**: 175-184.

[6] Zeng X, Xu C, Xu L. A method of improving the sensitivity of infrared to visible light conversion of temperature sensor based on Er^{3+} doped PLZT transparent ceramics. *J. Lumin.* 2019, **213**: 61-66.

[7] Wang X, Li X, Zhong H, et al. Up-conversion luminescence, temperature sensing properties and laser-induced heating effect of Er^{3+}/Yb^{3+} co-doped $YNbO_4$ phosphors under 1550 nm excitation. *Sci. Rep.* 2018, **8**: 5736-5749.

[8] Ma YJ, Zhu JL, Yang ZW, et al. Improving upconversion emission of $NaYF_4$: Yb^{3+}, Er^{3+} nanoparticles by coupling Au nanoparticles and photonic crystals: the detection enhancement of rhodamine B. *J. Alloy. Compd.* 2019, **788**: 1265-1273.

[9] Xu W, Zhang ZG, Cao WW. Excellent optical thermometry based in short-wavelength upconversion emissions in Er^{3+}/Yb^{3+} codoped $CaWO_4$. *Opt. Lett.* 2012, **37**: 4865-4867.

[10] Zheng H, Xiang SY, Chen BJ. Laser irradiation induced temperature effect of $NaY(WO_4)_2$: Tm^{3+}/Yb^{3+} using Er^{3+} as optical temperature sensors. *Chin J Lumin.* 2014, **35**: 800-806.

[11] Li K, Zhang Y, Li XJ, et al. Host-sensitized luminescence in $LaNbO_4$: Ln^{3+} (Ln^{3+}=Eu^{3+}/Tb^{3+}/Dy^{3+}) with different emission colors. *Phys. Chem. Chem. Phys.* 2015, **17**: 4283-4293.

[12] Singh AK, Singh SK, Gupta BK, et al. Probing a highly efficient mode: down-upconversion luminescence and temperature sensing performance of rare-earth oxide phosphors. *Dalton Trans.* 2013, **42**: 1065-1072.

[13] Tian YY, Tian Y, Huang P, et al. Effect of Yb^{3+} concentration on upconversion luminescence and temperature sensing behavior in Yb^{3+}/Er^{3+} co-doped $YNbO_4$ nanoparticles prepared via molten salt route. *Chemical Engineering Journal* 2016, **297**: 29-34.

[14] Liu X, Lü Y, Chen C, et al. Synthesis and luminescence properties of $YNbO_4$: A (A = Eu^{3+} and/or Tb^{3+}) nanocrystalline phosphors via a sol-gel process. *J. Phys. Chem. C* 2014, **118**: 27516-27524.

[15] Kaurya A, Yadac RS, Yadav RV, et al. Enhanced green upconversion photoluminescence from Ho^{3+}/Yb^{3+} co-doped $CaZrO_3$ phorsphor via Mg^{2+} doping. *RSC Adv.* 2016, **6**: 113469-113477.

[16] Prachur AK, Prasad AI, Rai SB, et al. Improvement of blue, white and NIR emissions in YPO_4: Dy^{3+} nanoparticles on co doping of Li^{3+} ions. *Dalton Trans.* 2012, **41**: 13810-13814.

[17] Yang M, Sui Y, Wang S, et al. Effects of Bi^{3+} doping on the optical properties of Er^{3+}: Y_2O_3. *J. Alloy. Compd.* 2011, **509**: 827-830.

[18] Sun WZ, Li HY, Zheng B, et al. Electronic structure and photoluminescence

properties of a novel single-phased color tunable phosphor $KAlGeO_4$: Bi^{3+}, Eu^{3+} for WLEDs. *J. Alloy. Compd.* 2019, **774**: 477-486.

[19] Xiao X, Yan B. Hybrid precursors synthesis and optical properties of $LnNbO_4$:Bi^{3+} blue phosphors and Bi^{3+} sensitizing of on Dy^{3+}'s luminescence in $YNbO_4$ matrix. *J. Alloy. Compd.* 2006, **421**: 252-257.

[20] Niu N, He F, Gai S, et al. Rapid microwave reflux process for the synthesis of pure hexagonal $NaYF_4$: Yb^{3+}, Ln^{3+}, Bi^{3+} (Ln^{3+} = Er^{3+}, Tm^{3+}, Ho^{3+}) and its enhanced UC luminescence. *J. Mater. Chem.* 2012, **22**: 21613-21623.

[21] Toby BH. EXPGUI, a graphical user interface for GSAS. *J. Appl. Cryst.* 2001, **34**: 210-213.

[22] Larson AC, Dreele RBV. Los Alamos National Laboratory Report LAUR. 1994, 86-748.

[23] Shannon RD. Revised effective ionic radii and systematic studies of interatomic distances in halides and chalcogenides. *Acta. Cryst. A.* 1976, **32**: 751-767.

[24] Chen G, Liu H, Liang H, et al. Upconversion emission enhancement in Yb^{3+}/Er^{3+}-codoped Y_2O_3 nanocrystals by tridoping with Li^+ ions. *J. Phys. Chem. C* 2008, **112**: 12030-12036.

[25] Ma Q, Lu MK, Yuan ZM, et al. Synthesis and photoluminescence of highly enhanced green-emitting $LaNbTiO_6$: xEr^{3+}, yBi^{3+} micro/nanophosphors. *Mater. Res. Bull.* 2012, **47**: 4126-4130.

[26] Sun W, Li H, Zheng B, et al. Electronic structure and photoluminescence properties of a novel single-phased color tunable phosphor $KAlGeO_4$: Bi^{3+}, Eu^{3+} for

WLEDs. *J. Alloy. Compd.* 2019, **774**: 477-486.

[27] Zhao WY, Qi SM, Lin J, et al. Luminescence properties and energy transfer of a color-tunable Y_2GeO_5: Bi^{3+}, Eu^{3+} phosphor. *J. Alloy. Compd.* 2019, **787**: 469-475.

[28] Xiang SY, Chen BJ, Zhang JS, et al. Microwave-assisted hydrothermal synthesis and laser-induced optical heating effect of $NaY(WO_4)_2$: Tm^{3+}/Yb^{3+} microstructures. *Opt. Mater. Express* 2014, **4**: 1966-1980.

[29] Wang X, Li XP, Cheng LH, et al. Concentration-dependent spectroscopic properties and temperature sensing of $YNbO_4$: Er^{3+} phosphors. *RSC Adv.* 2017, **7**: 23751-23758.

[30] Yadav RS, Kumar D, Singh AK, et al. Effect of Bi^{3+} ion on upconversion-based induced optical heating and temperature sensing characteristic in the Er^{3+}/Yb^{3+} co-doped La_2O_3 nano-phosphor. *RSC Adv.* 2018, **8**: 34699-34711.

[31] Yadav RS, Dhoble SJ, Rai SB. Improved photon upconversion photoluminescence and intrinsic optical bistability from rare earths co-doped lanthanum oxide phosphor via Bi^{3+} doping. *New. J. Chem.* 2018, **42**: 7272-7282.

[32] Shinn MD, Sinley WA, Drexhage MG, et al. Optical transitions of Er^{3+} ions in fluorozirconate glasses. *Phys. Rev. B* 1983, **27**: 6635-6648.

[33] Tripathi G, Rai VK, Rai SB. Upconversion and temperature sensing behavior of Er^{3+} doped Bi_2O_3-Li_2O-BaO-PbO tertiary glass. *Opt. Mater.* 2007, **8**: 201-206.

[34] Judd BR. Optical absorption intensities of rare-earth ions. *Phys. Rev.* 1962, **127**: 750-761.

[35] Ofelt GS. Intensities of crystal spectra of rare-earth ions. *J. Chem. Phys.* 1962, **37**:

511-520.

[36] Zhang YQ, Chen BJ, Xu S, et al. A universal approach for calculating Judd-Ofelt parameters of RE^{3+} in powdered phosphors and its application for β-$NaYF_4$: Er^{3+}/Yb^{3+} phosphor derived from auto-combustion assisted fluoridation. *Phys. Chem. Chem. Phys.* 2018, **23**: 15876-15883.

[37] Zhang YQ, Chen BJ, Xu S, et al. Reply to the 'Comment on "A universal approach for calculating the Judd-Ofelt parameters of RE^{3+} in powdered phosphors and its application for the b-$NaYF_4$: Er^{3+}/Yb^{3+} phosphor derived from auto-combustion-assisted fluoridation"' by D. Zhang, Q. Xu and Y. Zhang, Phys. Chem. Chem. Phys., 2019, 21, DOI: 10.1039/C8CP07577H. *Phys. Chem. Chem. Phys.* 2019, **21**: 10840-10845.

[38] Wang X, Li XP, Shen RS, et al. Optical transition and luminescence properties of Sm^{3+}-doped $YNbO_4$ powder phosphors. *J. Am. Ceram. Soc.* 2020, **103**: 1037-1045.

[39] Kortum G. Reflectance spectroscopy: principles, methods, applications, translated from the german by J. E. Lohr. *Springer-Verlag New York Inc* 1969, ISBN-13:978-3-642-88073-5.

[40] Luo WQ, Liao JS, Li RF, et al. Determination of Judd-Ofelt intensity parameters from the excitation spectra for rare-earth doped luminescent materials. *Phys. Chem. Chem. Phys.* 2010, **12**: 3276-3282.

[41] Sergio FLL, Ulises RRM, Atricia HGP, et al. Role of the host matrix on the thermal sensitivity of Er^{3+} luminescence in optical temperature sensors. *Sensor Actuat B-Chem* 2012, **174**: 176-186.

Figures

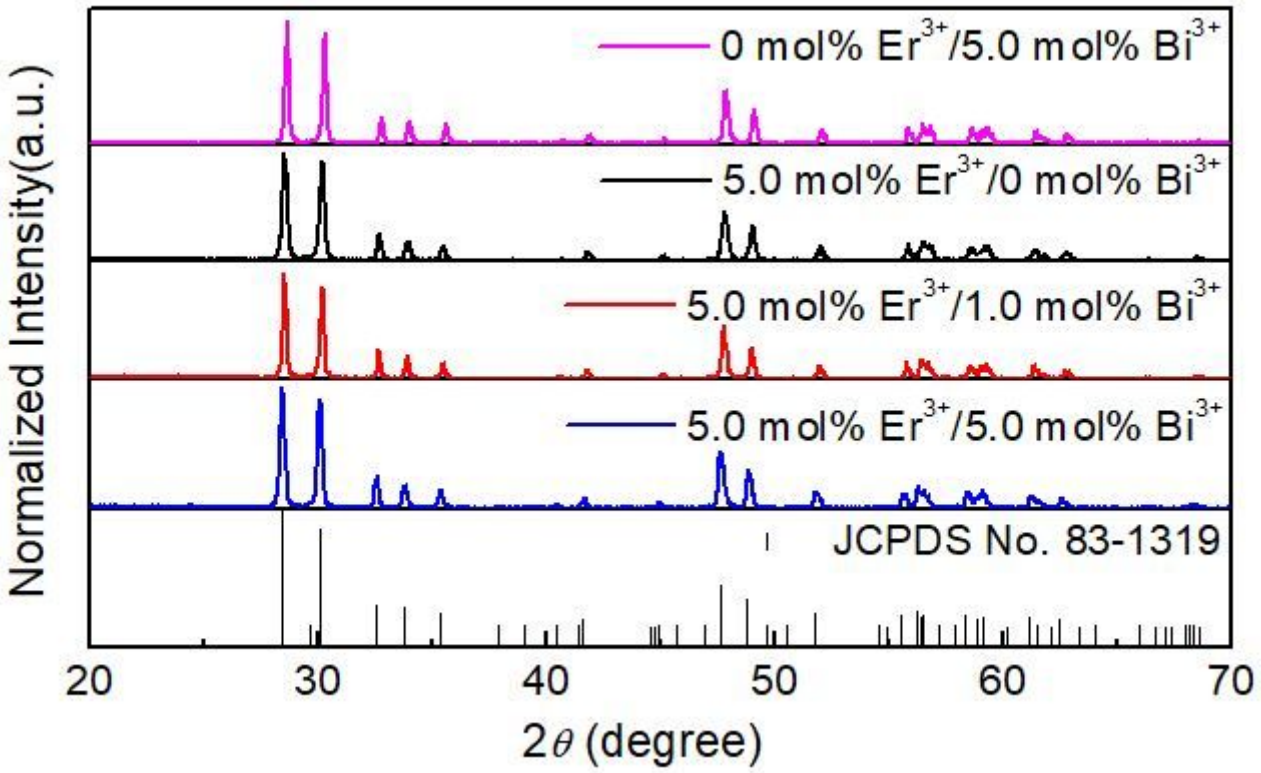

Figure 1

XRD patterns for 5.0 mol% Bi3+ single-doped and 5.0 mol% Er3+/x mol% Bi3+ (x = 0, 1.0, and 5.0) co-doped YNbO4 powders, together with the standard pattern of monoclinic YNbO4 plotted by using the data reported in JCPDS No. 83-1319.

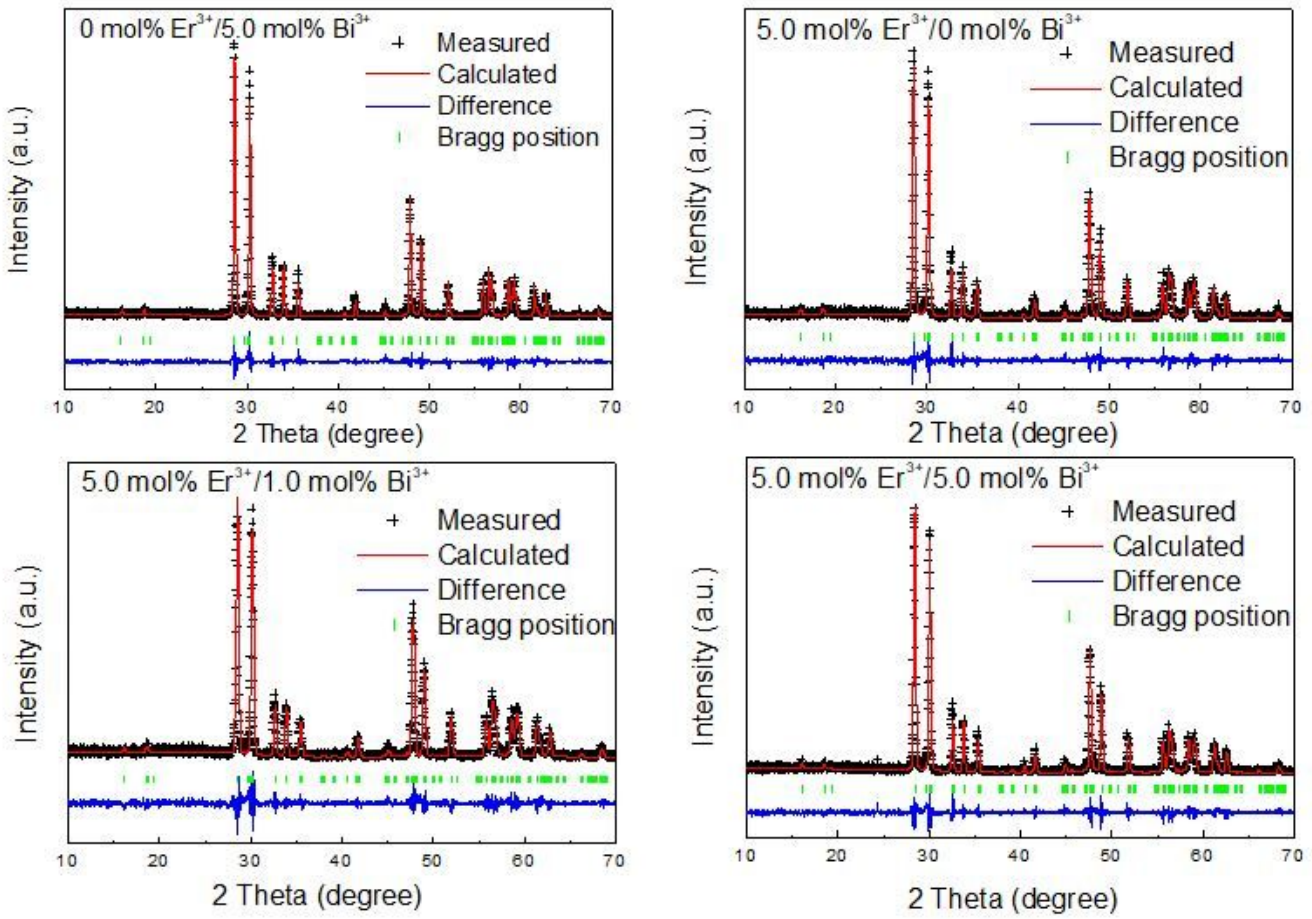

Figure 2

Rietveld refinement patterns for 5.0 mol% Bi3+ single-doped and 5.0 mol% Er3+/x mol% Bi3+ (x = 0, 1.0, and 5.0) co-doped YNbO4 powder phosphors.

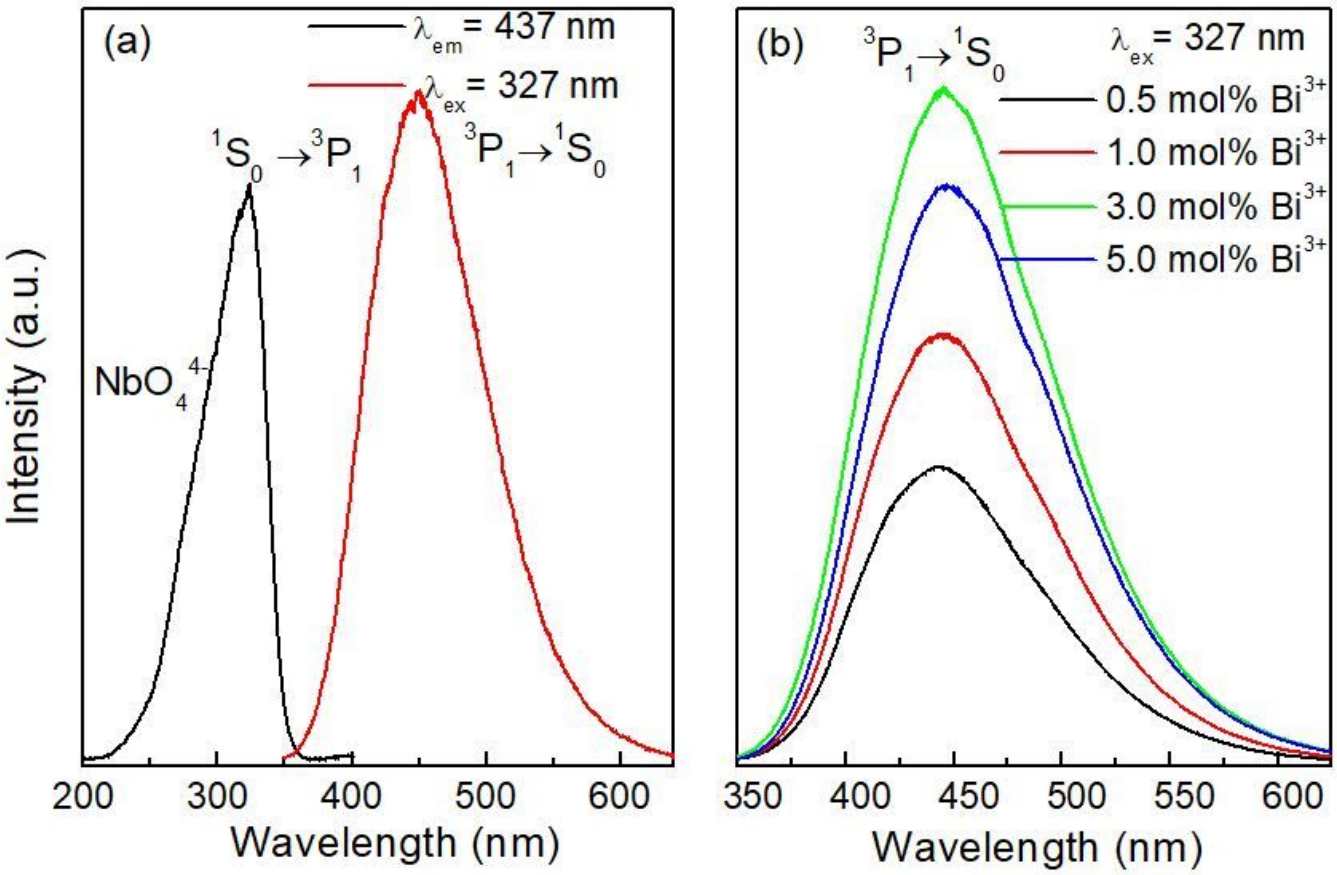

Figure 3

(a) Emission and excitation spectra of Bi3+ single-doped YNbO4 phosphor; (b) Emission spectra of YNbO4: Bi3+ phosphors with various concentrations of Bi3+ ions excited at 327 nm.

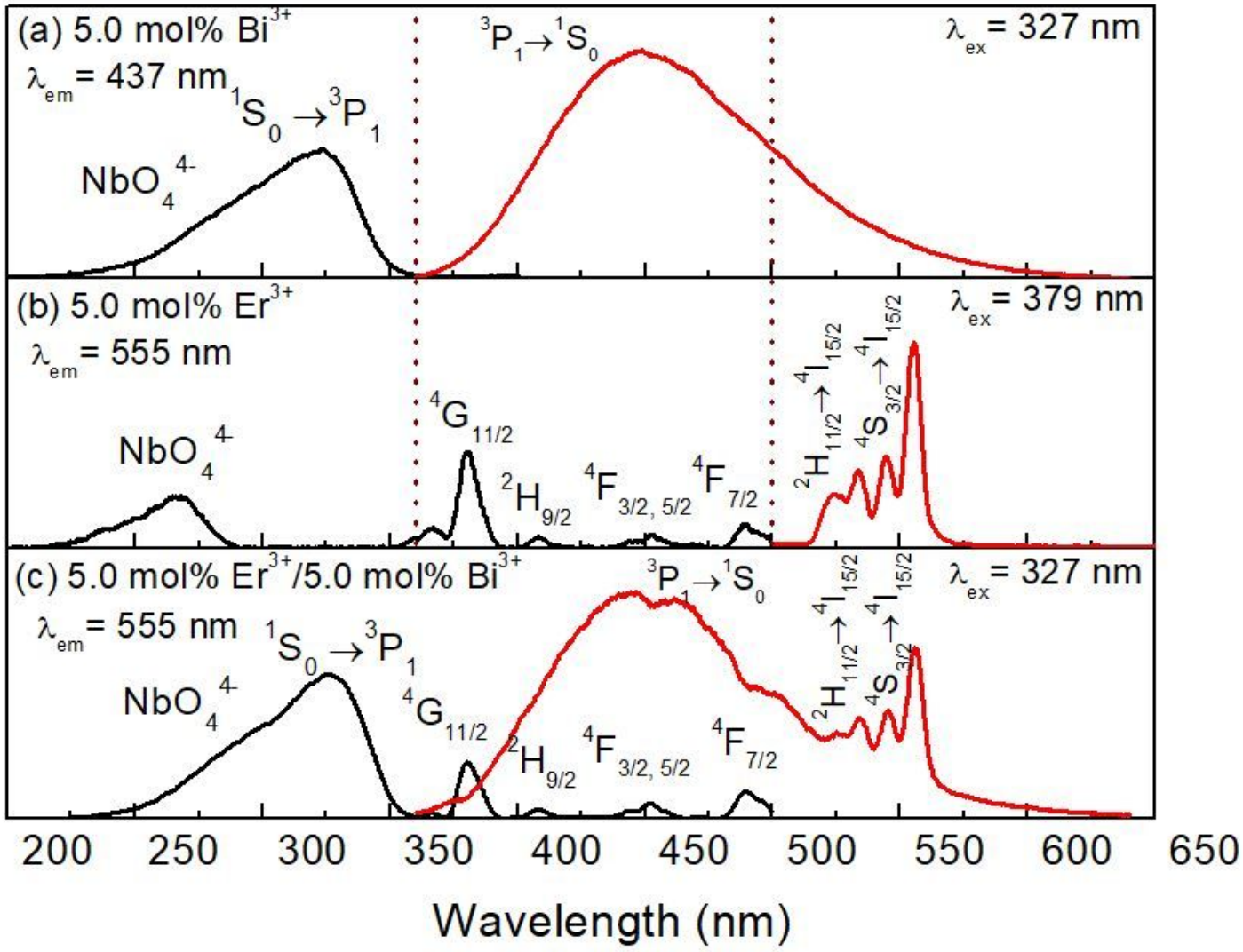

Figure 4

Excitation and emission spectra for 5.0 mol% Bi3+, 5.0 mol% Er3+ single-doped and co-doped YNbO4 samples.

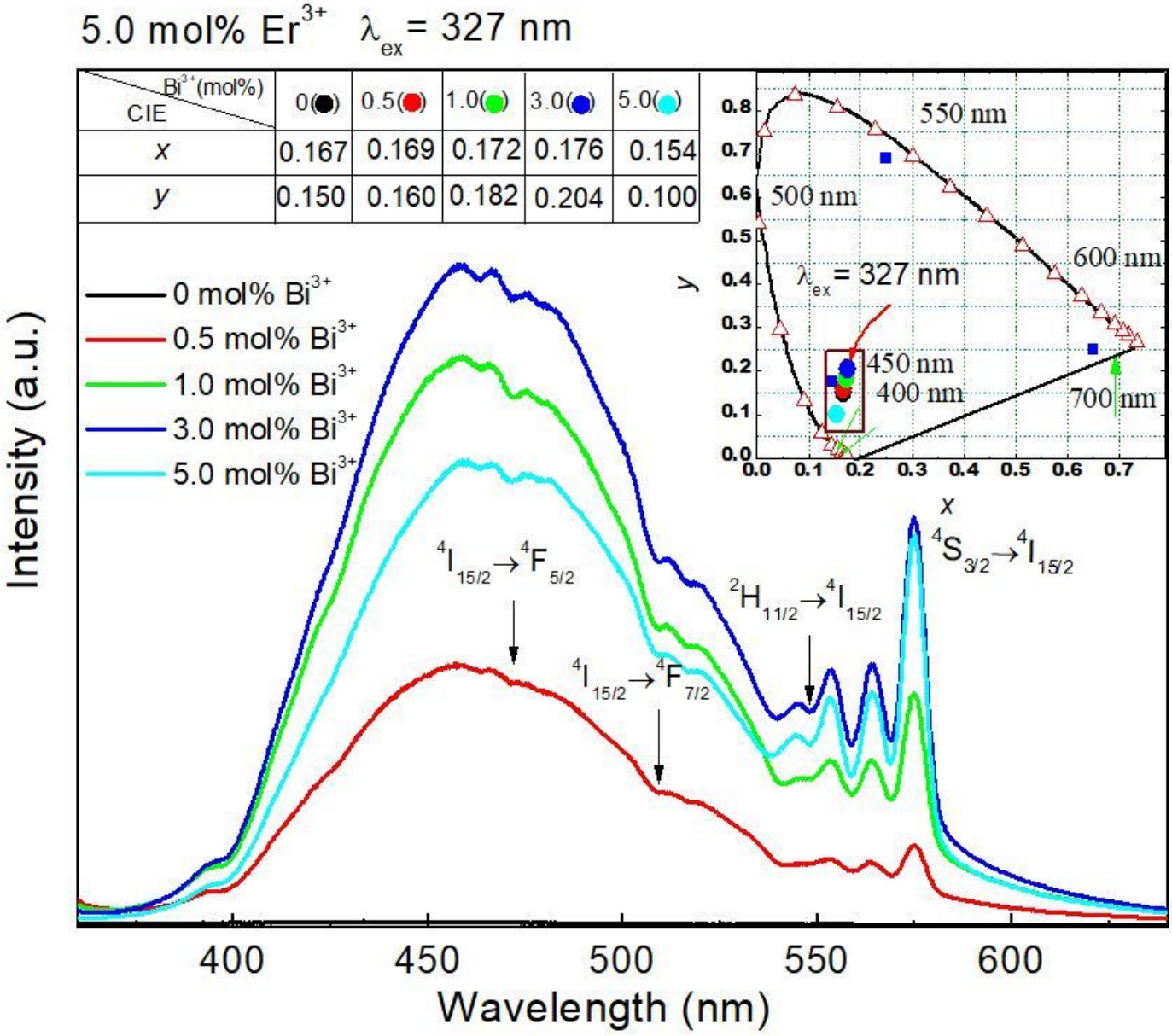

Figure 5

Emission spectra and the CIE color coordinates (the inset) of Er3+/Bi3+ co-doped YNbO4 phosphors excited at 327 nm.

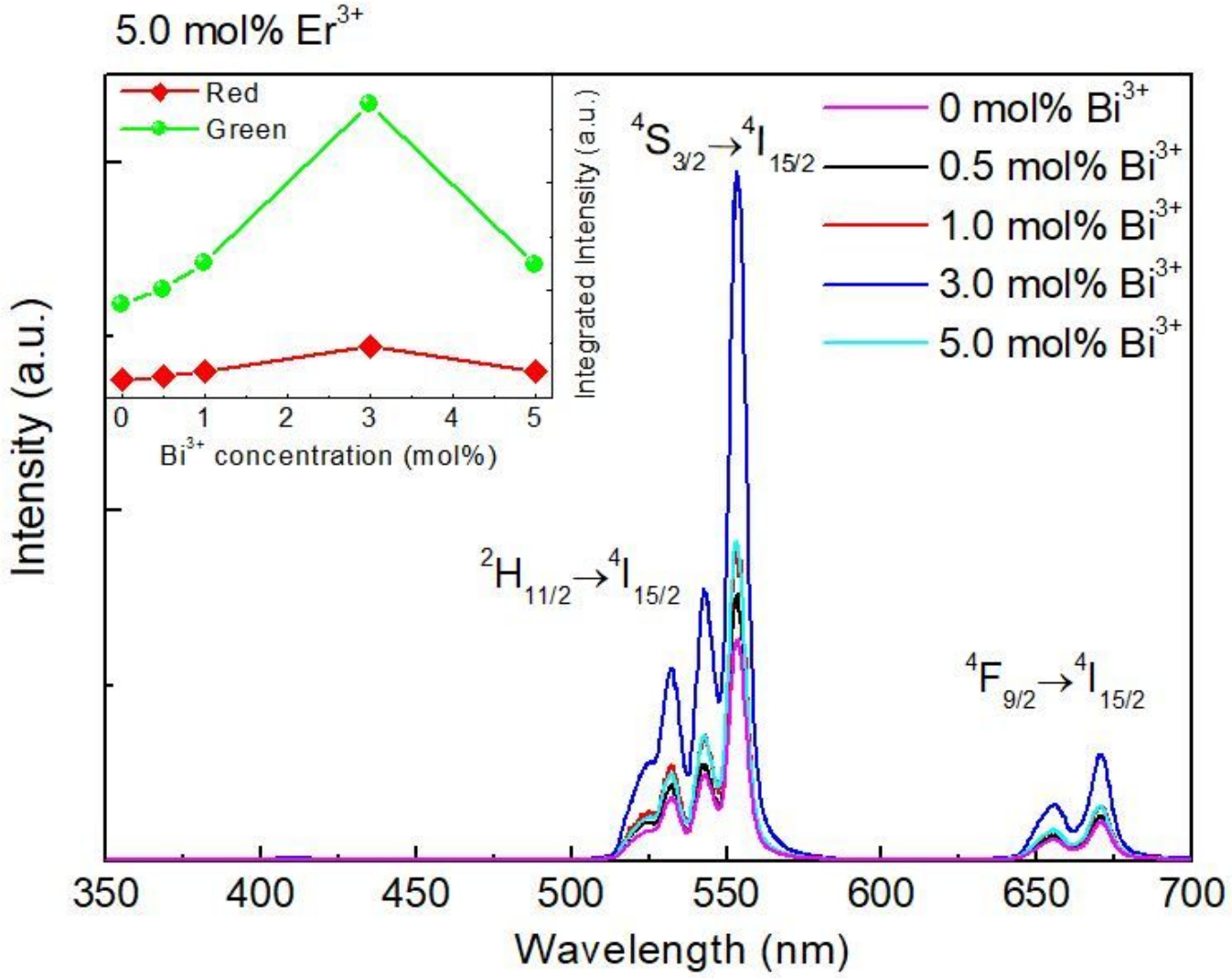

Figure 6

UC emission spectra of YNbO4: Er3+ phosphors doped with various concentrations of Bi3+ ions upon 980 nm excitation. The inset shows the dependence of the green and the red UC emission intensities on Bi3+ concentration.

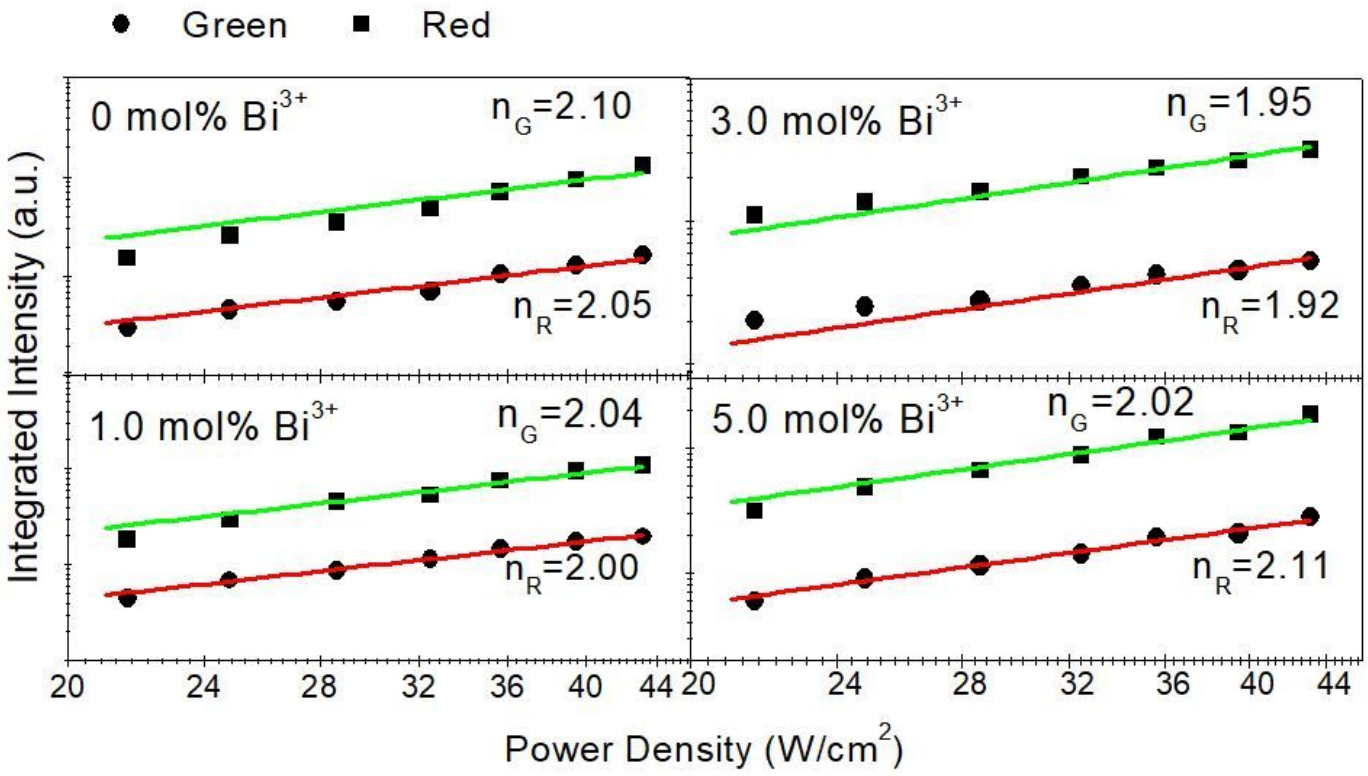

Figure 7

Dependence of the green and the red UC luminescence intensities on the excitation power density for YNbO4: Er3+/x mol% Bi3+ (x = 0, 1.0, 3.0, 5.0) samples.

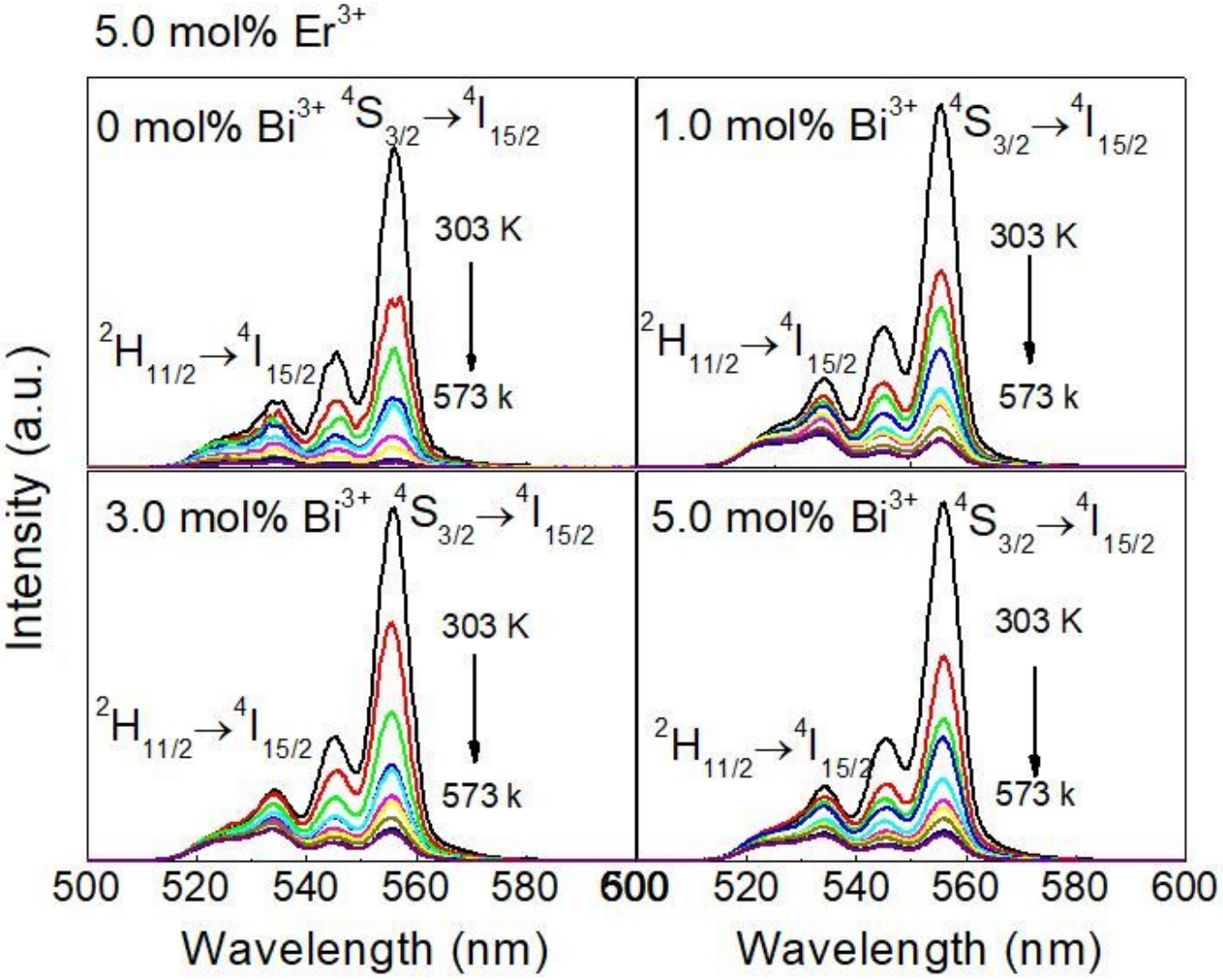

Figure 8

Temperature-varied UC luminescence spectra for YNbO4: Er3+/x mol% Bi3+ (x = 0, 1.0, 3.0 and 5.0) under 980 nm excitation.

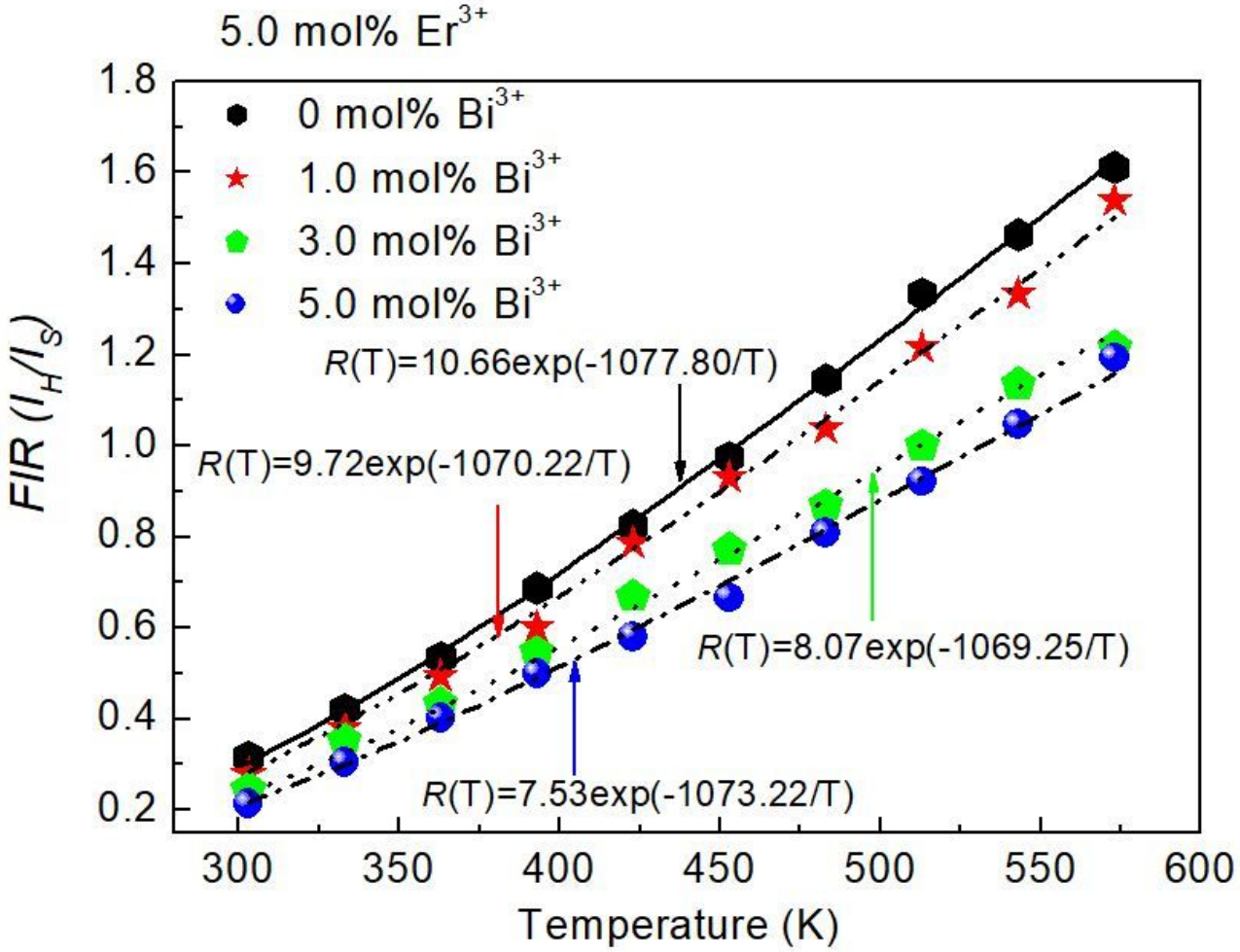

Figure 9

Temperature dependent FIR of the two green emissions of Er3+ ions in YNbO4: Er3+/x mol% Bi3+ (x = 0, 1.0, 3.0 and 5.0) on temperatures excited by 980 nm laser.

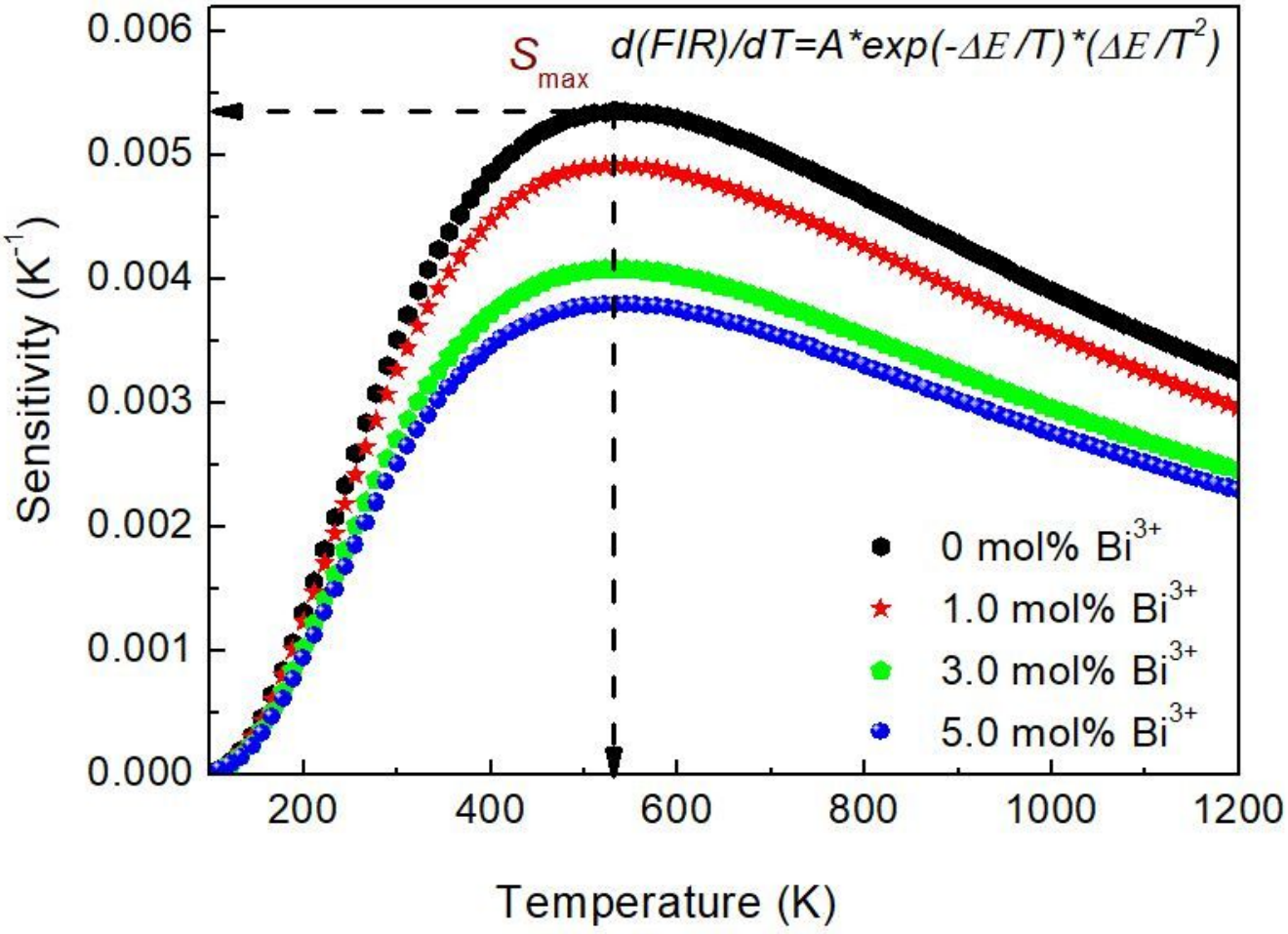

Figure 10

Temperature sensitivity curves of YNbO4: Er3+/x mol% Bi3+ (x = 0, 1.0, 3.0 and 5.0) under 980 nm excitation.

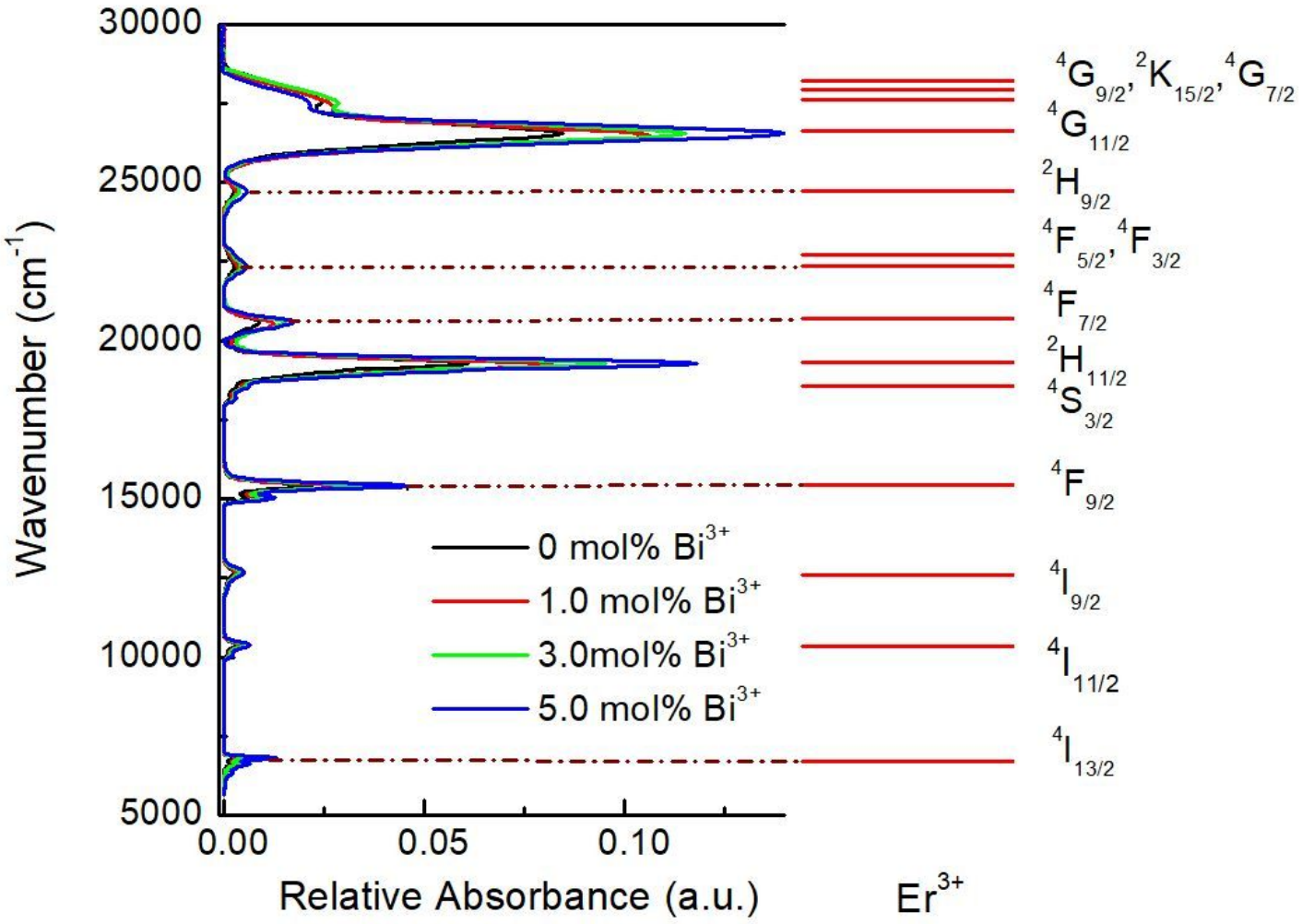

Figure 11

Relative absorption cross-section spectra of YNbO4: Er3+/x mol% Bi3+ (x = 0, 1.0, 3.0 and 5.0) phosphors.

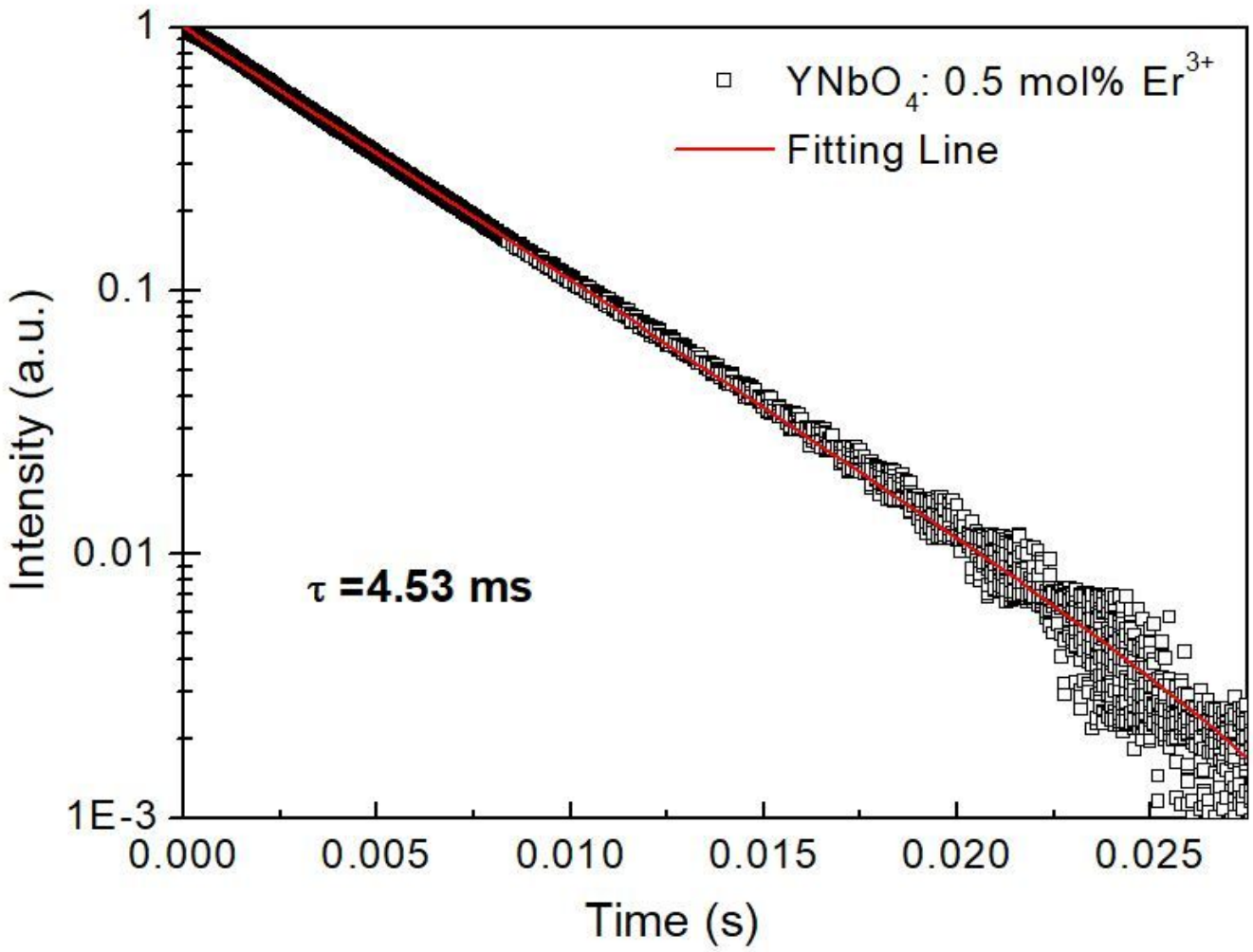

Figure 12

Fluorescence decay of 4I13/2 level in YNbO4: 0.5 mol% Er3+ phosphor.

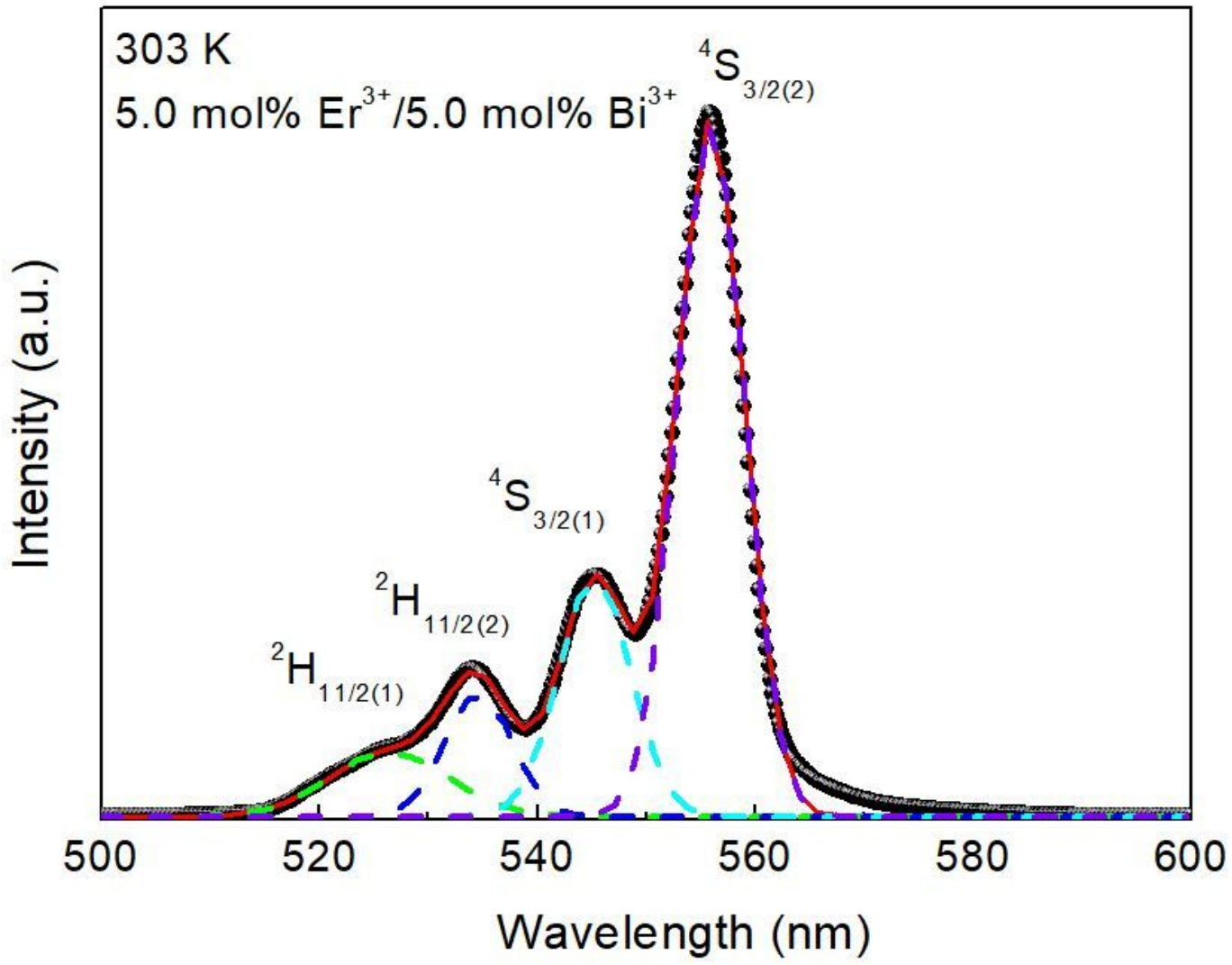

Figure 13

Gaussian peak fitting for (2H11/2, 4S3/2)→4I15/2 transitions for YNbO4: 5.0 mol% Er3+/5.0 mol% Bi3+ at 303 K.

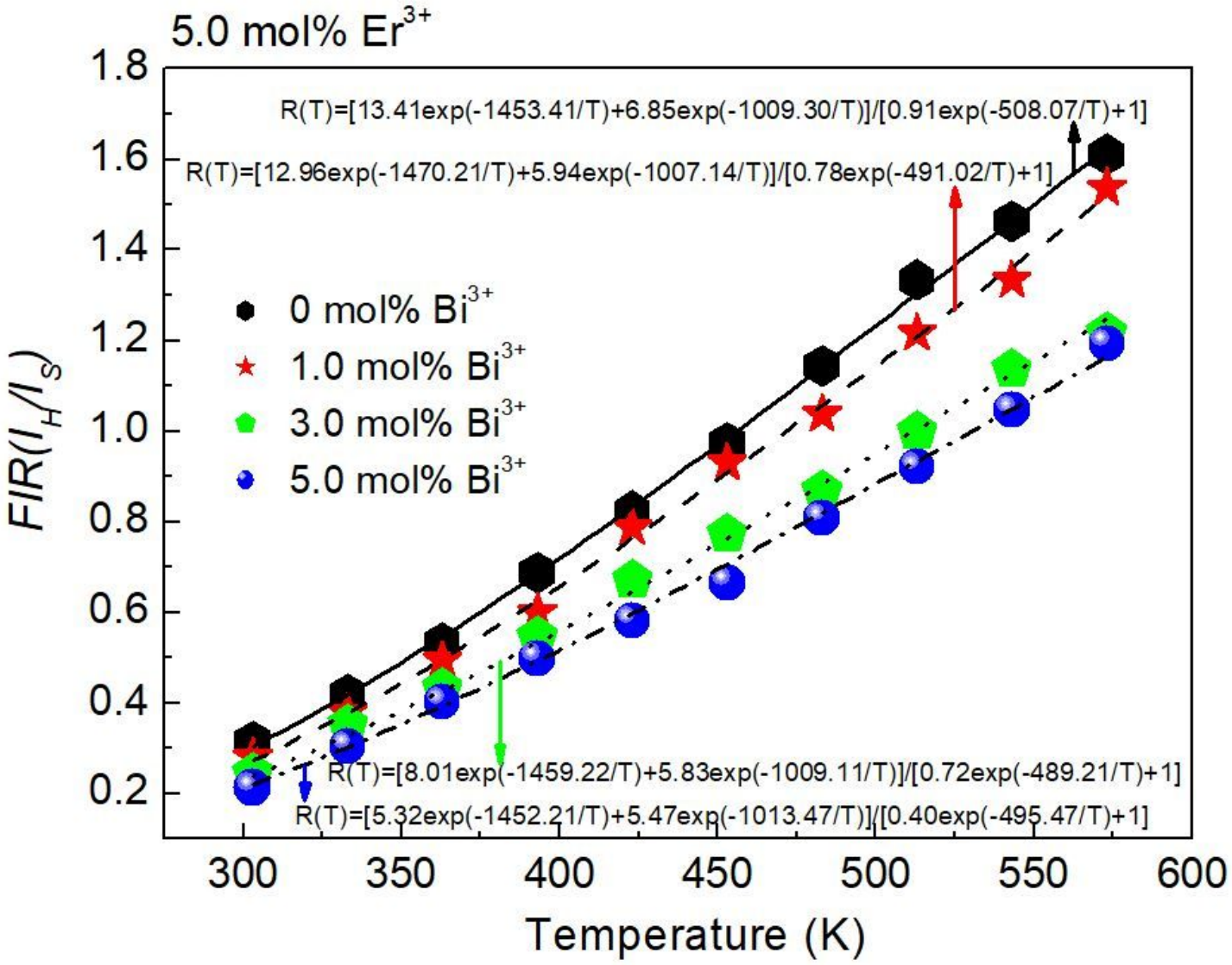

Figure 14

Temperature dependent FIR (R'(T)) of the two green emissions of Er3+ ions in YNbO4: Er3+/x mol% Bi3+ (x = 0, 1.0, 3.0 and 5.0) on sample temperatures.

Supplementary Files

This is a list of supplementary files associated with this preprint. Click to download.

- Table.docx
- Table.docx